

In-situ electron microscopy of the phases of Cu_3Si

Cheng-Yen Wen & Frans Spaepen*

Harvard School of Engineering and Applied Sciences, Cambridge, MA 02138 USA

The transformations between the η and η' phases of Cu_3Si were studied by *in-situ* transmission electron microscope (TEM) diffraction analysis and by differential scanning calorimetry (DSC). The space groups of η and η' are $P\bar{3}m1$ and $R\bar{3}$, respectively. The lattice parameters of η are $a = 4.06 \text{ \AA}$ and $c = 7.33 \text{ \AA}$. The η' phase results from faulted stacking of the η unit cell, and has lattice parameters: $a = 35.16 \text{ \AA}$ and $c = 21.99 \text{ \AA}$. A long-period anti-phase domain structure appears in these two phases and is part of a sequence of phase transformations from η' to η upon heating. The Cu silicide precipitates that form in voids in silicon are the η' phase, oriented in the silicon matrix according to: $(0001)_{\eta'} \parallel (110)_{\text{Si}}$; $[11\bar{2}0]_{\eta'} \parallel [001]_{\text{Si}}$.

Keywords: Cu_3Si ; Allotropes; Ordering; Long-period anti-phase domain; *in-situ* TEM; Calorimetry

1 Introduction

The aim of this study is to determine the crystal structure of the Cu silicide precipitates that fill voids [1]. The structural models of the Cu silicide precipitates in silicon crystals have been suggested to be $\beta\text{-Cu}_{85}\text{Si}_{15}$ [2], fcc-CuSi [3], and $\eta''\text{-Cu}_3\text{Si}$ [4], but these structures as well as other available Cu-Si structures can not satisfactorily explain the electron diffraction results

*Corresponding author. Email: spaepen@seas.harvard.edu

of the Cu silicide precipitates in our work. η'' -Cu₃Si is one of the three stable Cu-Si alloys at room temperature and is the most commonly observed phase in Cu-Si thin film reactions [5]. We found many similarities between our diffraction results and the crystal model of the η'' -Cu₃Si phase, which motivated us to undertake a detailed study of the structure of this alloy.

The Cu₃Si phase has three polymorphs, η , η' , and η'' . The transformation temperatures depend strongly on composition. For a Cu-24 at.% Si alloy, the current phase diagram [6] shows that η'' is stable at room temperature and transforms to η' at 531°C; the latter transforms to the η phase at 600°C. Each of these transition temperatures varies by as much as 100°C over the few percent stability range of the alloy composition. We will show that the $\eta' \rightarrow \eta$ transformation is more complex than currently understood.

The first complete structure analysis of the polymorphs of the Cu₃Si phase was performed by Solberg [4]. He analyzed the electron diffraction patterns of the Cu₃Si precipitates in silicon at room temperature. Inspired by the suggestion of a trigonally deformed body-centered cubic (b.c.c.) lattice in Cu₃Ge, he proposed that the η phase has a disordered trigonal unit cell, with space group $R\bar{3}m$ and lattice parameters $a_\eta=2.47 \text{ \AA}$ and $\alpha_\eta = 109.74^\circ$. His η' phase is an ordered phase of η , with space group $R\bar{3}$ and lattice parameters $a_{\eta'}=4.72 \text{ \AA}$ and $\alpha_{\eta'} = 95.72^\circ$. His η'' phase is a two-dimensional long-period superlattice of the η' unit cell, with lattice constants of $a_{\eta''}=76.76 \text{ \AA}$, $b_{\eta''}=7.00 \text{ \AA}$, and $c_{\eta''}=21.94 \text{ \AA}$. To estimate the composition of the precipitate he uses the area of the bounding dislocation loop, the total volume of the precipitates, and the average atomic volume of the precipitate phase, based on Nes's repeated nucleation model [7]. There is a large uncertainty in this method, so that the exact number of the atoms in the unit cell is not known.

In this work, a Cu-24 at.% Si alloy, which is within the composition range of all the polymorphs of the Cu₃Si phase [6], was synthesized for structure analysis. The crystal structures

of the polymorphs of the Cu-24 at.% Si alloy that will be proposed are based on the high temperature *in-situ* TEM diffraction analysis. A new long-period anti-phase domain (LPAPD) structure in this alloy system was discovered. The diffraction patterns of the Cu-24 at.% Si phases were used to identify the structure of the precipitates in the voids, which were shown to be the η' phase.

2 Experiments

A Cu-24 at.% Si film, 250 nm thick, was deposited by co-sputtering of Si and Cu on Si substrates. The composition was measured with Rutherford backscattering spectroscopy (RBS). TEM specimens for the *in-situ* analysis were prepared out of the as-deposited thin film. The silicon substrate was removed by ion beam (5 keV Ar⁺) polishing and the Cu silicide thin film was free-standing, which had the advantage that the stoichiometry of the thin film was constant during the high temperature annealing in the TEM. Furthermore, strong reflections from the silicon substrate, which may lead to complicated multiple scattering, were avoided.

In-situ electron diffraction analysis was performed in a field emission TEM, JEOL 2010F, operated at 200 kV, using a hot-stage holder (Gatan, model 652) that was calibrated by observing the formation of the Au-Si and Al-Si eutectic liquids [8]. The as-deposited Cu-24 at.% Si film consists of nanocrystals (<50 nm). The specimen was pre-heated at 750°C for 20 min, until the grains coarsened to about 1 μ m and kept a stable morphology in further heating. Twin planes are frequently seen inside the grains. These defects were carefully avoided when performing the selected-area diffraction (SAD) analysis. In SAD patterns, each reflection was examined in the two-beam condition to check whether it resulted from multiple diffraction or not.

The convergent-beam electron diffraction (CBED) method was used to obtain the point group symmetry of the structures. The spot size used in the CBED analysis was 1.6 nm, so

that the twin planes were easily avoided. Due to the thermal motion of the crystal lattice at high temperature, diffraction from the higher-order Laue zone is lost. Therefore, the symmetry of a unit cell must be determined more carefully by collecting the CBED patterns along several zone axes.

A bulk Cu-24 at.% Si alloy was synthesized from the weighed elements in an RF induction furnace with negligible weight loss. It was used for measuring the bulk properties of the alloy, such as the lattice constants by X-ray powder diffraction (XRD), the enthalpy of the phase transformations by DSC (Perkin Elmer Pyris 1), and the density. The density of the alloy was measured by comparing the weight of the alloy in air and in water. The synthesized Cu-24 at.% Si alloy was homogenized at 840°C for 24 h in flowing argon before the above measurements were made.

The SAD patterns of the Cu silicide precipitates in the silicon crystals were taken in several crystallographic orientations. After careful removal of the reflections due to multiple scattering, the extracted diffraction patterns of the precipitates were used to determine their crystal structure. The method to make the Cu silicide precipitates in silicon is described in the preceding paper [1].

3 Results

3.1 *Structure of the η phase*

For *in-situ* TEM diffraction analysis, the Cu-24 at.% Si thin film was heated to 750°C, which is in the η stability region of the phase diagram, and the SAD patterns of grains along different zone axes were recorded as shown in Fig. 1. The angular relations of the zone-axis patterns, the vector lengths and the relative intensities of the reflections in each pattern all agree with a hexagonal unit cell. Weak satellite spots appear around the reflections in Fig. 1. These satellite reflections are generated by the long-period anti-phase domains, as will be

discussed in Sec. 3.2.

Fig. 2(a) is the CBED pattern along the $[0001]_\eta$ axis. The pattern has 3-fold symmetry with three mirror planes parallel to the $\{11\bar{2}0\}_\eta$ planes. Only three point groups with 3m symmetry of their whole patterns have a hexagonal unit cell: $3m$, $\bar{3}m$, and $\bar{6}m2$. The intensity distribution in the pattern in Fig. 2(b) shows that it has two-fold rotational symmetry. In the above three point groups only $\bar{3}m$ has a 2-fold symmetry axis that is not parallel to the mirror plane. Therefore, the point group of the η phase is $\bar{3}m$. The mirror planes in Fig. 2(a) are confirmed by Figs. 2(c) and 2(d). The mirror symmetry is present parallel to the $\{11\bar{2}0\}_\eta$ plane. For the point group $\bar{3}m$ with mirror planes parallel to $\{11\bar{2}0\}$ planes, possible space groups are $P\bar{3}m1$, $P\bar{3}c1$, $R\bar{3}m$ and $R\bar{3}c$ [9]. If the space group is $R\bar{3}m$ or $R\bar{3}c$, the $\{1\bar{1}00\}$ reflections in Fig. 1(a) are forbidden. If the space group is $P\bar{3}c1$, the reflections of $(1\bar{1}0l)$, $l \neq 2n$, n is an integer, in Fig. 1(b) are forbidden. Therefore, the space group of the η phase is $P\bar{3}m1$.

It will be shown that all the polymorphs of Cu_3Si are composed of similar structural units, so that the coefficients of thermal expansion of the polymorphs are probably similar. The values of the composition and density found for the room temperature stable phase η'' can, therefore, be used for the η phase. It was also found that the c/a ratio of η is independent of the temperature: the ratio of the vector lengths of the reflections $(0002)_\eta$ and $(11\bar{2}0)_\eta$ in Fig. 1(b) does not change after the transformations from η to η'' . Therefore, the plane spacings obtained from X-ray powder diffraction analysis of the Cu-24 at.% Si alloy in the η'' structure can be used to calculate the lattice parameters of the hexagonal η unit cell. The two strongest diffraction peaks at 44.57° and 45.14° , representing $(11\bar{2}0)_\eta$ and $(1\bar{1}03)_\eta$, respectively, were used for the calculation; the results are $a=4.06 \text{ \AA}$ and $c= 7.33 \text{ \AA}$. The average c/a ratio is 1.81. The c/a ratio measured in *in-situ* SAD ranges between 1.78 and 1.84, which implies that the compositions of the Cu_3Si grains are slightly different,

in agreement with the existence of the Cu concentration range in the phase diagram. The density of the η'' phase was measured to be 7.36 ± 0.06 g/cm³, which corresponds to 6.33 Cu atoms and 2 Si atoms in the η unit cell. The non-integer atom number can be interpreted as a Cu atom dissolved interstitially in three unit cells, each of which has a structure composed of 6 Cu and 2 Si atoms. It can also be interpreted as two vacancies on the Cu sites of three unit cells, which have a structure composed of 7 Cu and 2 Si atoms. An alloy phase with composition of Cu-25 at.% Si (i.e. 6 Cu and 2 Si) is not stable over the temperature range we studied: on a bulk sample of this composition, we observed a liquid phase on the surface at a temperature around 840°C. Therefore, the structural model of the η phase is assumed to be a hexagonal unit cell that contains 7 Cu and 2 Si atoms with vacancies randomly distributed on the Cu sites.

The intensity distribution of the reflections in the SAD patterns may be complicated by dynamic scattering of the electrons. Therefore, the XRD spectrum of the η'' phase was used for the intensity analysis. As a result of ordering transformations, which involve rearrangement of the atom positions, the relative intensities of the reflections of the η phase change in the η' or η'' phases. However, the difference between the reflections of the η phase and those of the η' and η'' phases is not large [10], so that the relative intensities of the diffraction peaks in the XRD spectrum of the room temperature η'' phase can be used to verify the structural model of the η phase.

The International Tables [9] list as possible atom positions of the η phase consistent with the space group and the number of atoms (with Wyckoff notations): Cu at $1a$ (0,0,0); $2c$ (0,0, $\frac{1}{3}$) (0,0, $\frac{2}{3}$); $2d$ ($\frac{1}{3}, \frac{2}{3}, \frac{1}{6}$) ($\frac{2}{3}, \frac{1}{3}, \frac{5}{6}$); $2d$ ($\frac{1}{3}, \frac{2}{3}, \frac{1}{2}$) ($\frac{2}{3}, \frac{1}{3}, \frac{1}{2}$); and Si at $2d$ ($\frac{1}{3}, \frac{2}{3}, \frac{5}{6}$) ($\frac{2}{3}, \frac{1}{3}, \frac{1}{6}$); they are plotted in Fig. 3. These positions were also found to give the best fit (in which shifts in the z-direction were tested) to the relative intensities of the main diffraction peaks in the XRD spectrum of the η'' phase. A computed XRD spectrum of the η phase using RIETAN-2000

for the above structural model with the 90% occupancy at the Cu sites (which matches the stoichiometry of 6.33 Cu and 2 Si atoms in the Cu-24 at.% Si alloy) shows good agreement with the experimental data.

3.2 The structure and formation of the long-period anti-phase domain structure

The formation of the LPAPD appears to be a gradual process in the η phase region. The intensities of the satellite spots become stronger at lower temperature. On the other hand, the high temperature condition in which η exists without the LPAPD structure was never reached. When the specimen in the TEM was cooled down below 560°C, another set of superlattice reflections was present, representing the appearance of η' . The LPAPD reflections remained in the diffraction pattern and also occurred on the new superlattice reflections until the temperature was below 540°C, so that the LPAPD structure extends from the η phase to the η' phase.

The image of the LPAPD structure in a Cu-24 at.% Si grain at 750°C is shown in Fig. 4(a). The periodicity of the fringes is about 8 η hexagonal unit cells. These fringes are parallel to the $(0001)_\eta$ plane, which means that the hexagonal η building units are stacked along the $[0001]_\eta$ direction. The SAD pattern of the domain structure and the corresponding schematic illustration are shown in Figs. 4(b) and 4(c), respectively. Due to the existence of the LPAPD, the $(hk \cdot l)_\eta$ reflection, with $h - k = 3m$, is forbidden at $l = 2n + 1$, where m and n are integers, e.g. $(0001)_\eta$ and $(0003)_\eta$. Apart from the reflections of the η phase, LPAPD reflections, $(hk \cdot l)_{SL}$, are forbidden when l is an even number. Some of them, such as $(00 \cdot 2)_{SL}$, $(00 \cdot 14)_{SL}$, and $(00 \cdot 18)_{SL}$ etc., appear due to multiple diffraction. Unlike the other close-packed cubic alloys with anti-phase domain structures, such as CuAu and Cu₃Pd [11, 12], which show satellite reflections only around the forbidden reflections, satellite spots occur around both

the forbidden and allowed reflections in the η phase, as shown in Fig. 4(c).

The spacing between the two satellite spots around the $(0001)_\eta$ reflection, $(00\cdot7)_{SL}$ and $(00\cdot9)_{SL}$, is the reciprocal of the average domain size, which is 4.1 times the lattice constant c of the η unit cell, as measured in Fig. 4(b). Therefore, on average, each domain is composed of 4.1 η unit cells along the c -axis with the same phase and adjoins another domain of the same size but with a phase shift. The incommensurate domain size of 4.1 unit cells may result from an average of nine domains consisting of four unit cells and one domain consisting of five unit cells [13]. For the sake of simplicity, a domain with four unit cells is used to index the superlattice reflections in Fig. 4(c).

A $(000l)_\eta$ reflection is forbidden when $l = 2n + 1$, so that there is a phase shift of π between two adjacent domains along the $[0001]_\eta$ direction. The same phase shift should make all the reflections $(hk \cdot l)_\eta$ with $l \neq 2n$ vanish. However, among these reflections, only those with $h - k = 3n$ are not observed. Another phase shift of $2\pi(\frac{h}{3} - \frac{k}{3})$ between the two domains is therefore required to avoid the extinction of reflections such as $(1\bar{1}\cdot1)_\eta$ and $(1\bar{1}\cdot3)_\eta$ etc.. Based on the above rules and the structural model of the η phase, a possible anti-phase domain structure is proposed as illustrated in Fig. 5. The structure consists of two alternating domains that are shifted by a phase angle of $2\pi(\frac{h}{3} - \frac{k}{3} + \frac{l}{2})$ in their structure factors. Domain I in Fig. 5 is composed of 4 η unit cells. The atoms in domain II have been shifted by $\frac{\mathbf{a}}{3} - \frac{\mathbf{b}}{3} + \frac{\mathbf{c}}{2}$ with respect to those in domain I. As a result of the stacking of the two domains, the structure factor of the LPAPD structure is

$$F = F_I \sum_{n=0}^3 e^{2\pi i n l} + e^{2\pi i 4l} F_{II} \sum_{n=0}^3 e^{2\pi i n l} \quad (1)$$

where F_I and F_{II} are the structure factors of the η unit cells in domains I and II, respectively.

A phase shift of $2\pi(\frac{h}{3} - \frac{k}{3} + \frac{l}{2})$ is included in F_{II} .

Intensities of the reflections of the LPAPD structure were calculated with the CaRIne Crystallography program, which uses X-ray atomic scattering factors. The relative intensities along $(00\cdot l)_{SL}$ of the LPAPD reflections are listed in Table 1. The reflections of the η phase, such as $(00\cdot 8)_{SL}$ and $(00\cdot 24)_{SL}$ (corresponding to the forbidden reflections, $(0001)_{\eta}$ and $(0003)_{\eta}$, respectively), have zero intensity. Furthermore, the superlattice reflections that originated from the LPAPD structure have zero intensity when $l = 2n$. In the model, however, two Cu atoms (labeled by A and A' in Fig. 5) at the boundary between the two domains are too close together to be both present. As mentioned earlier, vacancies exist in the η structure, and they can replace either Cu atom. Calculation shows that the intensity distribution is closest to that in the SAD pattern when a vacancy randomly replaces one of the two Cu atoms. The relative intensities of the LPAPD structure with vacancies at the domain boundary are also listed in Table 1. Such a modification breaks the selection rules described previously, but the intensities of the originally forbidden reflections ($l = 2n$) are still too low to be experimentally observed. The calculated intensities of the LPAPD structure are generally consistent with those in the TEM SAD patterns in Figs. 1 and 4(b), which in any case are only qualitatively known.

3.3 Structure analysis of the η' phase

The diffraction patterns of the single domain η' phase are shown in Figs. 6(a) and 6(c). New superlattice reflections of η' in Fig. 6(a) are located between $(000l)_{\eta}$ and $(11\bar{2}l)_{\eta}$ in Fig. 1(c) and those in Fig. 6(c) are between $(000l)_{\eta}$ and $(1\bar{1}0l)_{\eta}$ in Fig. 1(b). Without the existence of LPAPD, reflections at $(0001)_{\eta}$ and $(0003)_{\eta}$ are excited in the η' phase. In the *in-situ* observation, the intensities of the η reflections did not decrease while these new superlattice reflections were appearing. Therefore, the η' phase may be a faulted stacking of the η unit cells. When the temperature was below 400°C, the diffraction pattern in Fig. 6(d) appeared,

indicating the appearance of the η'' phase.

Figure 6(b) illustrates the reflections of the η' phase. The locations of the superlattice reflections in the $[0001]_\eta$ direction are at exact multiples of $\frac{1}{3}\mathbf{g}_{(0001)_\eta}$, but they are not rational fractions of the vector $\mathbf{g}_{(\bar{2}1\cdot0)_\eta}$. For example, the reflection labeled $(\bar{4}4\cdot1)_{\eta'}$ is located at $\frac{1}{3}\mathbf{g}_{(0001)_\eta}$, and the fraction along $\mathbf{g}_{(\bar{2}1\cdot0)_\eta}$ ranges between 0.266 and 0.289. The irrational fraction could have a cause similar to the one that produced the incommensurate domain size of the LPAPD: it is an average over several η' unit cells with slightly different domain size. The fraction 0.266 is close to the rational number $4/15$. Thus, the η' unit cell may contain fifteen $(\bar{2}110)_\eta$ planes when viewed in the $[\bar{2}110]_\eta$ direction. The occurrence of the reflections at the locations of $\frac{1}{3}\mathbf{g}_{(0001)_\eta}$ implies that the unit cell size along the $[0001]_\eta$ is three times the $(0001)_\eta$ plane spacing.

Consider a hexagonal layer as a stacking unit. Similar to the stacking of 3C SiC [14], if the second layer shifts $\frac{2}{3}\mathbf{a} + \frac{1}{3}\mathbf{b}$ relative to the first layer and the third layer has that same shift relative to the second layer, the diffraction conditions become: for the $(\bar{k}k \cdot l)$ reflections, if $k = 3n + 1$, the column of the reflections moves $\frac{1}{3}\mathbf{g}_{(0001)}$; if $k = 3n + 2$, the column of the reflections moves $\frac{2}{3}\mathbf{g}_{(0001)}$; if $k = 3n$, the reflections do not move. Due to the stacking, the unit cell becomes three times larger in the $[0001]$ direction. We can apply this relation to define the η' unit cell. In Fig. 7 the dashed lines are a drawing of the η unit cells in the $[0001]_\eta$ projection. The basal plane of the η' unit cell is represented by the thick lines. The $\mathbf{a}_{\eta'}$ axis is parallel to $[10\bar{1}0]_\eta$ and the $\mathbf{b}_{\eta'}$ axis is parallel to $[\bar{1}100]_\eta$. The η' unit cell contains fifteen $\{1\bar{2}10\}_\eta$ planes (represented by the thin lines in Fig. 7) parallel to its $\{10\bar{1}0\}$ planes, and the lattice parameter a is 35.16 \AA . Assume that a layer with a thickness of one η unit cell in the c direction is used as the stacking layer and that each stacking layer is shifted $\frac{2}{3}\mathbf{a}_{\eta'} + \frac{1}{3}\mathbf{b}_{\eta'}$ relative to previous layer. This stacking results in the shift of some of the diffraction spots as follows: the $(\bar{4}4\cdot l)_{\eta'}$ spots move $\frac{1}{3}\mathbf{g}_{(0001)_\eta}$; the $(\bar{8}8\cdot l)_{\eta'}$ spots move $\frac{2}{3}\mathbf{g}_{(0001)_\eta}$; the $(\bar{1}212 \cdot l)_{\eta'}$

spots do not move. The lattice parameter c of the η' unit cell hence becomes 21.99 \AA , three times that of the η unit cell. The reflections of the η' unit cell are indexed as shown in Fig. 6(b). The reflections of $\{\bar{k}k \cdot l\}$ with $k \neq 4n$ should vanish, except with $k = 15$, which are the reflections of the $\{\bar{2}1 \cdot 0\}_\eta$. However, the exact atom arrangement in the η' unit cell that can cause the extinction of those reflections has not been determined.

Figure 8 shows the CBED patterns of the η' phase. The pattern in Fig. 8(a) contains a 3-fold rotation axis. The pattern along the zone axis $[11\bar{2}0]_{\eta'}$ (along the white lines in Fig. 8(a)) shows 2-fold rotational symmetry (Fig. 8(b)), which is caused by a shift of $\frac{2}{3}\mathbf{a}_{\eta'} + \frac{1}{3}\mathbf{b}_{\eta'}$, so that the unit cell contains an inversion center. The point group of the η' phase is therefore $\bar{3}$. The indices in Fig. 6(b) satisfy the diffraction condition: $-h + k + l = 3n$, so that the space group of the η' phase is $R\bar{3}$ [9].

The structure of the η'' phase is more complicated as revealed in the SAD pattern of Fig. 6(d). The diffraction patterns of η' and η'' have similar strong reflections. The superlattice reflections in η'' also have an irrational vector length relative to the those of the η' phase. The streaking along the c -axis between diffraction spots indicates a stacking fault plane parallel to the $(0001)_{\eta'}$. The η'' phase may also result from faulted stacking of the η' structure.

3.4 *The structure of the precipitates*

The Cu silicide precipitates in the silicon voids are present as single domains; no planar defect was observed [1]. We can hence directly compare the diffraction patterns of the precipitates with those of the polymorphs of the Cu_3Si phase. When the multiple diffraction spots and the reflections from silicon in Fig. 9 are removed (see the schematic illustrations), the remaining patterns of the Cu silicide precipitate are similar to the diffraction patterns of the η' phase: the reflections from the precipitates in Figs. 9(a) and 9(c) are similar to those in the

$[11\bar{2}0]_{\eta'}$ and $[1\bar{1}00]_{\eta'}$ patterns (Figs. 6(a) and 6(c)), respectively. The superlattice reflections in Fig. 6(c) are relatively weak, so that they are not revealed in Fig. 9(c).

The angle between the two patterns in Figs. 9(a) and 9(c) is 90° , consistent with the orientation relation of the $[11\bar{2}0]_{\eta'}$ and $[1\bar{1}00]_{\eta'}$ zone-axis patterns, which can differ by 30° or 90° . The 30° angular relation was also found in the precipitate structure. When the precipitate in Fig. 9(c) was tilted by 30° about the $[220]_{Si}$ axis, the resulting diffraction pattern in Fig. 9(e) contains the $[11\bar{2}0]_{\eta'}$ zone-axis pattern, as in Fig. 6(a). Furthermore, the relative intensities of the reflections of the precipitates are close to those of the η' phase. Therefore, we conclude that the precipitates in the voids are the η' phase, rather than the equilibrium η'' phase. The orientation relation between the precipitate and the silicon matrix is: $(0001)_{\eta'} \parallel (110)_{Si}$; $[11\bar{2}0]_{\eta'} \parallel [001]_{Si}$. The above crystal structure and orientation relationship have been verified in the precipitates between 15 nm and 100 nm; no size-dependence of the crystal structure has been observed.

The size of the precipitates in the silicon voids is typically less than 100 nm [1]. The small size of the precipitates prevents the transformation from the η' phase to η'' . This size effect was also observed in the Cu-24 at.% Si grains in the TEM specimen. The original η'' grain in the thin area (<100 nm) of the specimen did not go back to the η'' structure after *in-situ* heating, but remained in the η' phase.

3.5 Phase transformations in Cu_3Si

The above results demonstrate the transformations of the Cu-24 at.% Si alloy, including the formation of the LPAPD structure. These transformations in a grain and the transition temperatures are reproducible in repeated heating cycles. The precise transition temperatures can not be determined directly in *in-situ* TEM experiments because of the composition-dependence of the transition temperatures and the limited accuracy of the temperature

read-out in the TEM hot-stage holder. Therefore, DSC was used to monitor the transformations in the bulk Cu-24 at.% Si alloy. In order to have a good signal-to-noise ratio, a large mass, typically around a hundred milligram, was used.

Figure 10(a) is a scan between room temperature and 730°C at a rate of 40 K/min. In the heating curve, there are two endothermic peaks with onset temperatures of about 470°C and 560°C. In the cooling curve, a split exothermic peak at 554°C and a smooth exothermic peak at around 400°C (onset temperature at 439.3°C) are observed. When a lower rate of 1 K/min was used in the temperature range between 530°C and 580°C, the endothermic peak at 560°C was resolved into two peaks, as shown in Fig. 10(b). In addition, the split peak at 554°C in the cooling curve of Fig. 10(a) became two distinct peaks. The heating cycles in the Fig. 10(b) show the correspondence of the two endothermic peaks in the heating curve to the two exothermic peaks in cooling curve. Similar heating cycles were applied to the endothermic peak at 470°C. Heating started from different temperatures and went up to 550°C at a rate of 40 K/min, as shown in Fig. 10(c). It indicates that the smooth exothermic peak at around 400 °C in the cooling curve in Fig. 10(a) corresponds to the endothermic peak at 470°C. In summary, there are three endothermic signals at 470°C, 556°C, and 563°C in the DSC heating curve. The first endothermic peak is assigned to the $\eta'' \rightarrow \eta'$ transformation. In light of the *in-situ* TEM diffraction analysis, the LPAPD forms in the η' phase upon heating, right before the η' phase transforms to the η phase, so that the second endothermic peak, at 556°C, is due to the formation of the LPAPD. The peak at 563°C is assigned to the transformation of the η' phase to the η phase.

Mima and Hasegawa studied the phase transformations in Cu₃Si by means of thermal analysis, electrical resistance measurements, and optical microscopic observation, and concluded that there were only two transformations, $\eta \rightarrow \eta'$ and $\eta' \rightarrow \eta''$, during cooling [15]. Their thermal analysis, however, also shows two endothermic peaks, which occurred at the $\eta' \rightarrow \eta$

transformation around 560°C. A similar heating curve was reported by Smith [16]. This phenomenon can be explained now by the incorporation of the LPAPD formation during the transformation of from η' to η .

The domain size of the LPAPD in an alloy is a function of the composition, in other words, the electron-atom ratio, and the temperature [12, 17, 18]. Figure 11 shows the domain size, in units of η unit cells, of three different grains measured from the satellite spacing in the *in-situ* TEM diffraction patterns as a function of temperature. When the temperature is lowered the domain size increases, so that the number of the interfaces between the domains decreases. The average domain size at temperatures higher than 650°C is about 4.2 η unit cells. The domain size increases abruptly to around 6 when the η' phase is formed in favor of the domain size equivalent to two η' unit cells, which contain three η unit cells along the [0001] axis.

According to Sato's theory [17, 19], formation of a LPAPD structure or of stacking fault boundaries electronically stabilizes the bulk alloy phase. This stabilization is balanced by the energy of the domain boundaries, which is a function of temperature. When the temperature is lowered, the number of the interfaces decreases or another stacking sequence forms in order to minimize overall free energy of the system. This can explain the sequential formation of the LPAPD in the η phase and the different stacking order in the η' phase with some overlap between the two. The transformation from η' to η'' probably occurs by a similar mechanism.

4 Discussion

The space group of the η phase is $P\bar{3}m1$, and there is no limitation on the reflections for diffraction [9]. Even if the Cu and Si atoms are distributed randomly among the positions in the unit cell, the reflections from this structure do not change, except for a slight variation in the relative intensity. However, random distribution of the atoms in the η unit cell can

not make the required phase shift that satisfies the extinction rules of the reflections with the LPAPD structure. Therefore, η is not a disordered structure, and the $\eta - \eta'$ boundary in the phase diagram does not simply indicate a disorder-order transformation.

An advantage of *in-situ* observation is that the diffraction patterns of the Cu-24 at.% Si phases at various temperatures can be obtained without ambiguity. The zone-axis patterns in Fig. 1 provide information for postulating the hexagonal unit cell of the η phase, and the discovery of the LPAPD structure further confirmed that the η phase is an ordered structure. If the structure of the high temperature η phase is postulated only from the diffraction pattern of the low temperature superlattice structure, based on the idea that strong reflections, e.g. $(0009)_{\eta'}$ in Fig. 6, are those inherited from a simple unit cell at high temperature, it may lead to the misinterpretation that the unit cell of the η phase has a c/a ratio of 0.61, which is close to a b.c.c. structure. Solberg used a slightly distorted b.c.c., or rhombohedral, unit cell to describe the disordered η phase [4]. In that structural model, the shortest reciprocal lattice vectors observed in the $[111]$ zone-axis pattern are the $\{1\bar{1}0\}$ reflections, which correspond to the $\{11\bar{2}0\}_{\eta}$ reflections in the equivalent zone-axis pattern in Fig. 1(a). As can be seen in the diffraction pattern, the $\{1\bar{1}00\}_{\eta}$ reflections are also present, so that the unit cell is better described as hexagonal. Structural models of the precipitates based on a cubic symmetry [2, 3] are hence not satisfactory.

El Kajbaji *et al.* reported the existence of disordered β -Cu₈₅Si₁₅ precipitates in the grain boundary and in the silicon lattice [2, 20]. They used high-resolution TEM (HRTEM) to measure the lattice spacings for structure analysis. From their results, plane spacings equivalent to those of the $(1\bar{1}03)_{\eta}$ and $(11\bar{2}0)_{\eta}$ planes were found. In addition, the angular relation between the two planes and orientation relation of the precipitate with the silicon matrix are both in agreement with our structural model of η' . Seibt also analyzed the HRTEM lattice fringes of the precipitates and proposed that the lattice of the precipitate should be close to

hexagonal [21]. In his results, the lattice spacing is 7.38 \AA along the c -axis, which coexists with another set of lattice planes with a spacing of 3.5 \AA . This lattice structure corresponds to the η' phase oriented along the zone axis of $[\bar{1}\bar{1}00]_{\eta'}$, so that the precipitate structure is also closely related to the η' phase. The structural model of the η phase also accounts for the above observations. However, η is a less stable phase than η' . In addition, the η phase is always accompanied by the LPAPD structure, but the LPAPD domain structure is not seen in the HRTEM images.

Solberg extracted the real reflections of the Cu silicide precipitates from the diffraction patterns by carefully removing those resulting from multiple scattering [4]. Figs. 3 and 6 in his article are very similar to the diffraction patterns of the η' phase along the $[11\bar{2}0]_{\eta'}$ in Figs. 6(a) and $[\bar{1}\bar{1}00]_{\eta'}$ Fig. 6(c), respectively, except that the superlattice reflections in Fig. 6(c) are not indicated, possibly because they are so weak. Even though Solberg claims to see η'' , we do not find our η'' pattern in his data. Therefore, the precipitate in Solberg's result is the η' phase rather than the η'' phase. The precipitates in the above three studies were produced by quenching the Cu-saturated silicon crystals from high temperature and, based on our understanding of the structures in the Cu_3Si system, they are likely in the metastable η' phase.

5 Conclusion

Three transformations between the polymorphs in Cu_3Si , $\eta'' \rightarrow \eta'$, the appearance of LPAPD in η' , and $\eta' \rightarrow \eta$, were observed *in-situ* in the TEM and the peaks in the DSC. The SAD and CBED results revealed a hexagonal unit cell in the η phase and space group $P\bar{3}m1$. From the XRD data of the Cu-24 at.% Si alloy, the lattice parameters of the η unit cell are $a = 4.06 \text{ \AA}$ and $c = 7.33 \text{ \AA}$. The density of the Cu-24 at.% Si alloy at room temperature was used to calculate the numbers of Si and Cu atoms in the η hexagonal cell, and a possible structural

model of the η phase was proposed. The η' phase is thought to result from a special stacking sequence of the η unit cell. Although the exact atom positions in the η' structure have not been determined, the unit cell is proposed to be hexagonal with lattice parameters $a = 35.16 \text{ \AA}$ and $c = 21.99 \text{ \AA}$. The space group of η' is $R\bar{3}$. An LPAPD structure was discovered, which can also be described as stacking of the η unit cells. The structure of the precipitates in the voids in Si was determined by comparing the electron diffraction patterns of all of the phases of the Cu-24 at.% Si alloy, and it is determined to be the metastable η' phase, with the orientation relation with the silicon matrix: $(0001)_{\eta'} \parallel (110)_{Si}$; $[11\bar{2}0]_{\eta'} \parallel [001]_{Si}$.

Acknowledgements

This work was supported by the National Science Foundation as a Cooperative Activity in Materials Science between NSF and the European Commission. We thank Xi Wang for his help with thin film deposition.

References

- [1] C. Y. Wen and F. Spaepen, preceding paper.
- [2] M. El Kajbaji, J. Dessus and J. Thibault, *Phil. Mag. A* **66** 873 (1992).
- [3] G. Das, *J. Appl. Phys.* **44** 4459 (1973).
- [4] J. K. Solberg, *Acta Cryst. A* **34** 684 (1978).
- [5] G. Weber, B. Gillot and P. Barret, *Phys. Stat. Sol. A* **75** 567 (1983).
- [6] T. B. Massalski, J. L. Murray, L. H. Bennett and H. Baker (Editors), *Binary Alloy Phase Diagrams* (American Society for Metals, 1986), pp. 960-963.
- [7] E. Nes, *Acta Metall.* **22** 81 (1974).
- [8] C. Y. Wen, Precipitation of Copper Silicide in Voids in Silicon Single Crystals. PhD thesis, Harvard University (2005).
- [9] N. F. M. Henry and K. Lonsdale (Editors), *International Tables for X-ray Crystallography, Vol. 1* (Kynoch Press, Birmingham, England, 1965).
- [10] K. P. Mukherjee, J. Bandyopadhyaya, and K. P. Gupta, *AIME Trans.* **245** 2335 (1969).
- [11] A. B. Glossop and D. W. Pashley, *Proc. Roy. Soc. (Lond) A* **250** 132 (1959).
- [12] S. Takeda, J. Kulik and D. de Fontaine, *J. Phys. F: Met. Phys.* **18** 1387 (1988).
- [13] K. Fujiwara, *J. Phys. Soc. Japan* **12** 7 (1957).
- [14] W. F. Knippenberg, *Philips Res. Repts.* **18** 161 (1963).
- [15] G. Mima and M. Hasegawa, *Technol. Rep. Osaka Univ.* **10** 157 (1960).
- [16] C. S. Smith, *AIME Trans.* **83** 414 (1929).
- [17] H. Sato and R. S. Toth, *Phys. Rev.* **124** 1833 (1961).

- [18] H. Sato and R. S. Toth, Phys. Rev. **127** 469 (1962).
- [19] H. Sato, R. S. Toth and G. Honjo, J. Phys. Chem. Solids **28** 137 (1967).
- [20] M. El Kajbaji and J. Thibault, Phil. Mag. Lett. **71** 335 (1995).
- [21] M. Seibt, Solid State Phenomena **19&20** 45 (1991).

Figure captions

Figure 1: Selected-area diffraction (SAD) patterns of the η phase at 750°C. The zone axis of (a) is normal to those of (b) and (c). The angle between the zone axes of (b) and (c) is 30° using $[0001]_\eta$ as a rotating axis, and that of (c) and (d) is 19.2° using $[11\bar{2}0]_\eta$ as a rotating axis. They are indexed as (a) $[0001]_\eta$, (b) $[11\bar{2}0]_\eta$, (c) $[1\bar{1}00]_\eta$, and (d) $[3\bar{3}01]_\eta$, using a hexagonal model. In (b), the reflections $(000l)$ are forbidden when l is not an even number. Their appearance is due to multiple scattering.

Figure 2: Convergent-beam electron diffraction (CBED) patterns of the η phase along (a) $[0001]_\eta$, (b) $[11\bar{2}0]_\eta$, (c) $[1\bar{1}00]_\eta$, and (d) $[3\bar{3}01]_\eta$. The CBED disks correspond to the respective strong reflections in Fig. 1. Mirror planes in the patterns are indicated by the white lines with symbol m.

Figure 3: (a) Structural model of the η phase. (b) Projection of the η structure along the $[2\bar{1}\bar{1}0]$ axis.

Figure 4: (a) Image of the long-period anti-phase domain (LPAPD) structure in a Cu-24 at.% Si grain at 750°C. (b) Part of the SAD pattern of the grain along $[11\bar{2}0]_\eta$. (c) Schematic illustration and indexation of the diffraction pattern: solid circles represent real reflections from the structure; open circles represent those due to multiple scattering. Two systems of the plane indices are used in (c): one is for the reflections of the η phase; the other system with subscript "SL" is used to index the diffraction planes of the LPAPD superlattice structure.

Figure 5: Structural model of the long-period anti-phase domains (LPAPD) in the η phase. Each domain consists of four unit cells. The η unit cells are stacking along the c -axis in domain I. In domain II, the atoms in each unit cell have been shifted $\frac{\mathbf{a}}{3} - \frac{\mathbf{b}}{3} + \frac{\mathbf{c}}{2}$ with respect

to the η unit cell in domain I, where \mathbf{a} , \mathbf{b} , and \mathbf{c} are the vectors defined in Fig. 3. One of the Cu atoms that are labeled by A and A' is randomly replaced by a vacancy.

Figure 6: (a) SAD pattern of η' along $[11\bar{2}0]_{\eta'}$ at 540°C. (b) Schematic illustration of the real reflections in (a). (c) SAD pattern of the η' phase along $[1\bar{1}00]_{\eta'}$ at 540°C. (d) SAD pattern of the η'' phase in the same orientation as in (c).

Figure 7: Orientation relation between the η' unit cell and the η unit cell.

Figure 8: CBED patterns of the η' phase at 450°C along (a) $[0001]_{\eta'}$ and (b) $[11\bar{2}0]_{\eta'}$.

Figure 9: SAD patterns of the precipitates along the zone axes of (a) $[1\bar{1}0]_{Si}$ and (c) $[001]_{Si}$. (e) SAD pattern obtained after tilting the precipitate in (a) 30° about the Si(220) axis. (b), (d), and (f) are the respective schematic illustrations.

Figure 10: Heat flow as a function of temperature for a Cu-24 at.% Si alloy. (a) Endothermic and exothermic signals during heating and cooling at a rate of 40 K/min. (b) Heating cycles at 1 K/min in the temperature range between 530°C and 580°C, showing two endothermic peaks and the corresponding exothermic peaks. (c) Heating cycles at 40 K/min with a starting temperature between 380°C and 420°C, showing the corresponding endothermic and exothermic peaks. The exothermic peaks in (c) are very broad and difficult to distinguish.

Figure 11: Temperature-dependence of the domain size of the LPAPD structure, as measured in the *in-situ* TEM SAD patterns. The dashed line indicates the transition temperature between the η and η' phases.

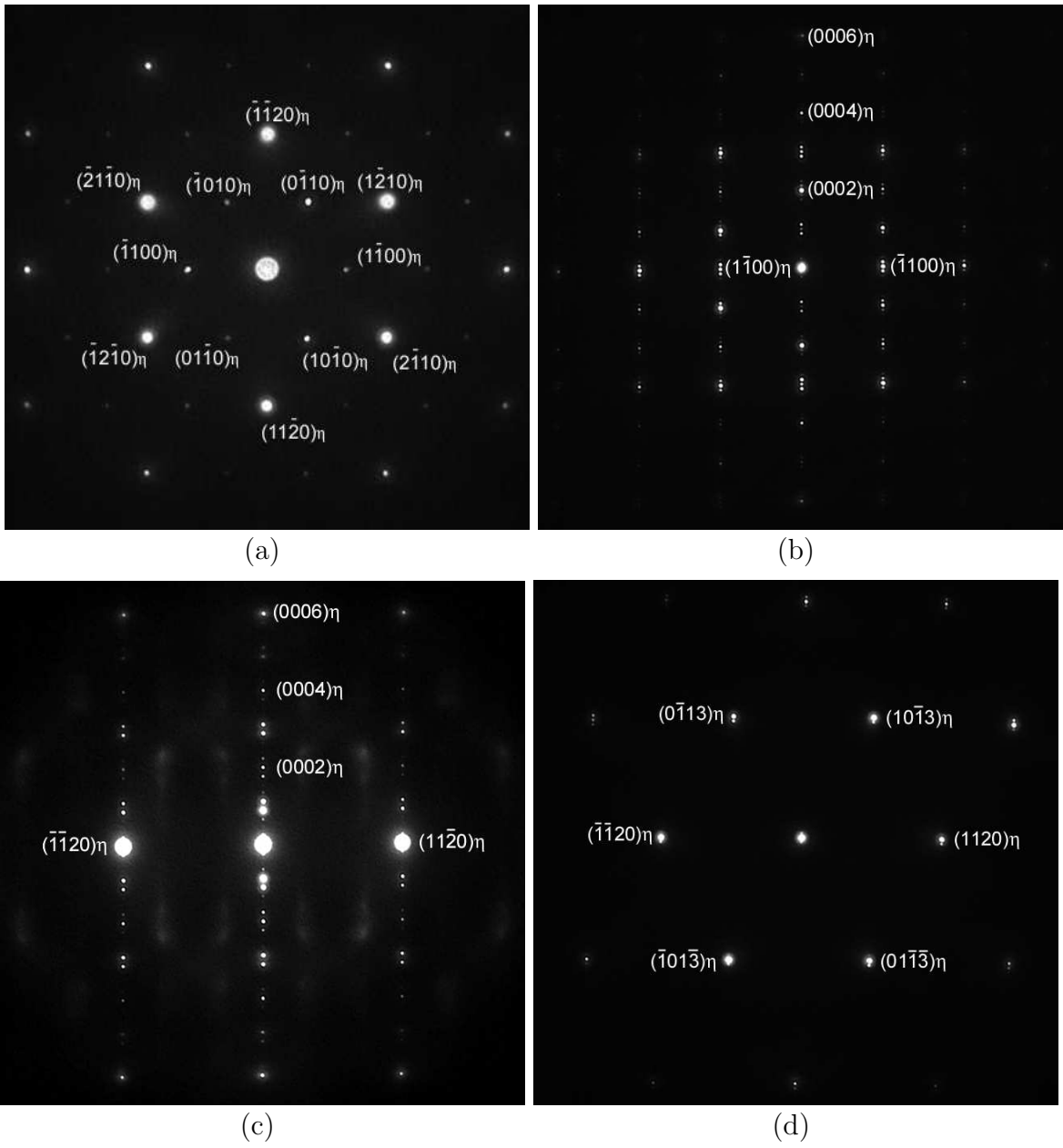
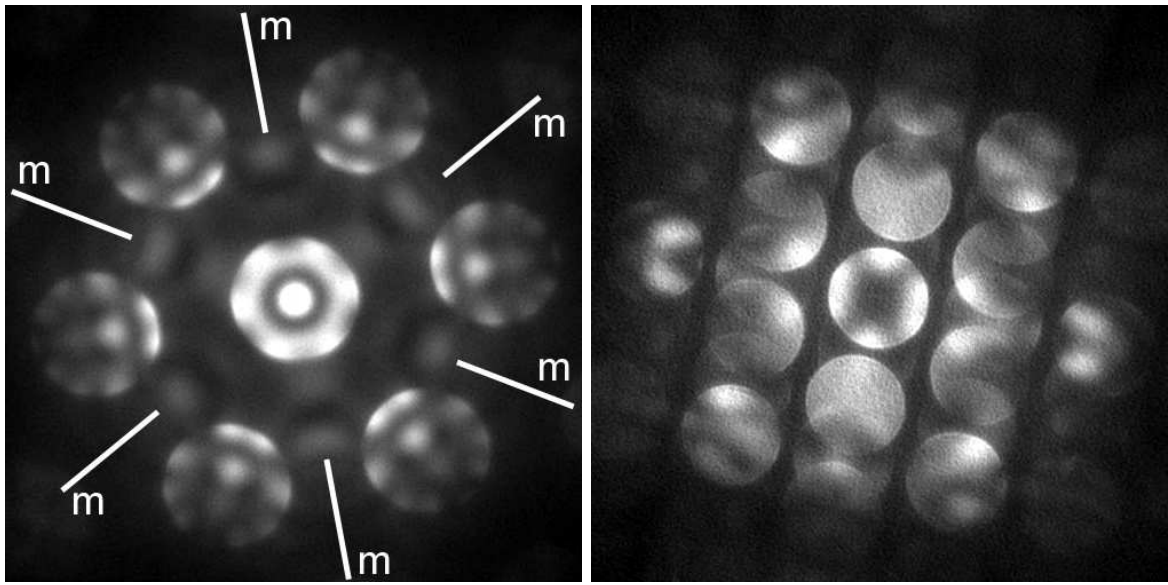
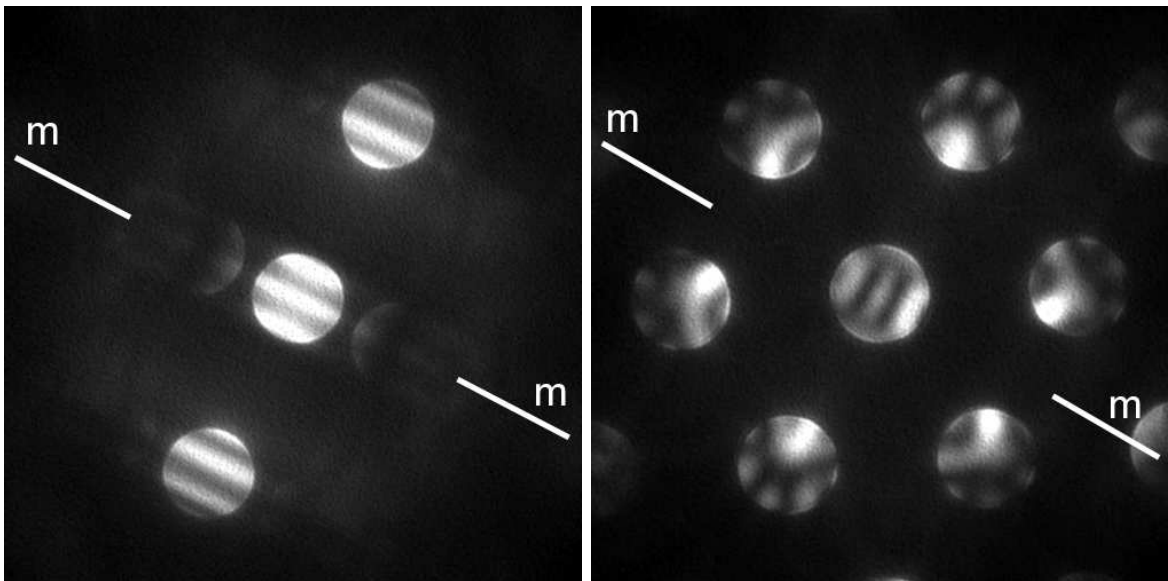


Figure 1.



(a)

(b)



(c)

(d)

Figure 2.

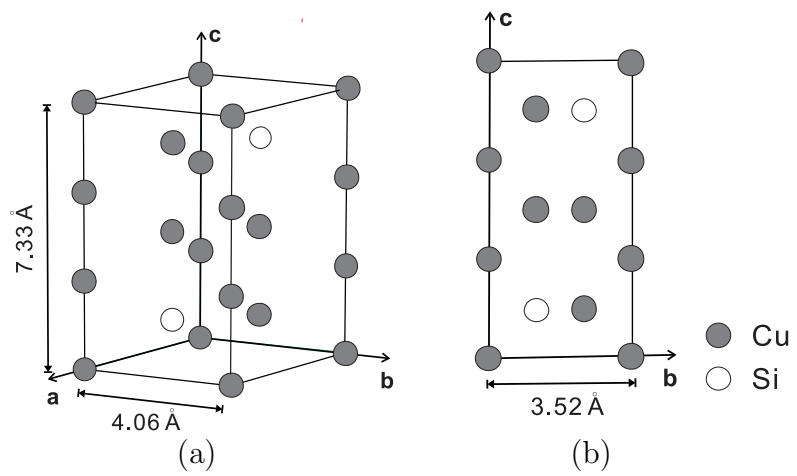
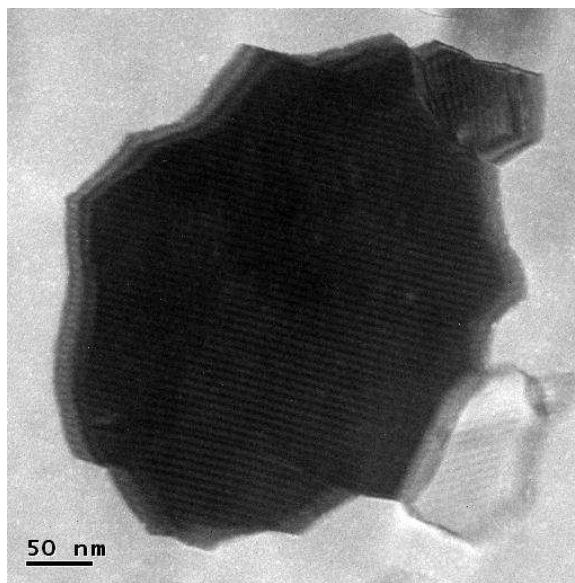
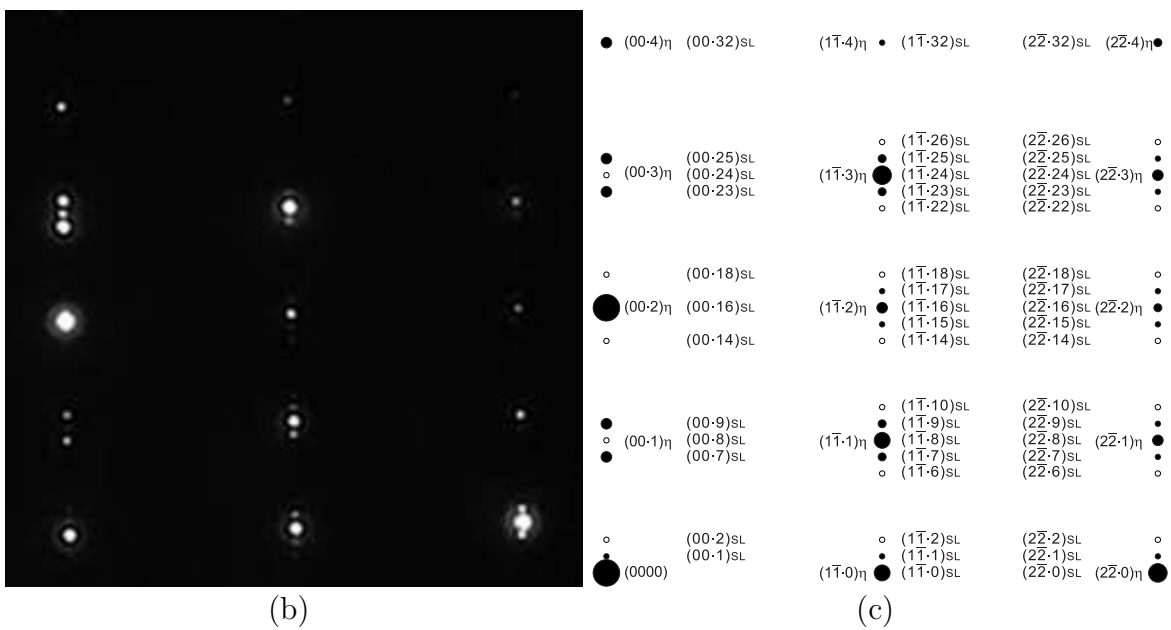


Figure 3.



(a)

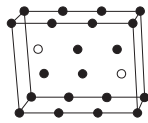


(b)

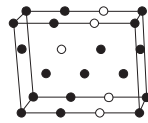
(c)

Figure 4.

η unit cell in domain I



η unit cell with $a/3-b/3+c/2$ shift in domain II



• Cu
○ Si

The LPAPD structure

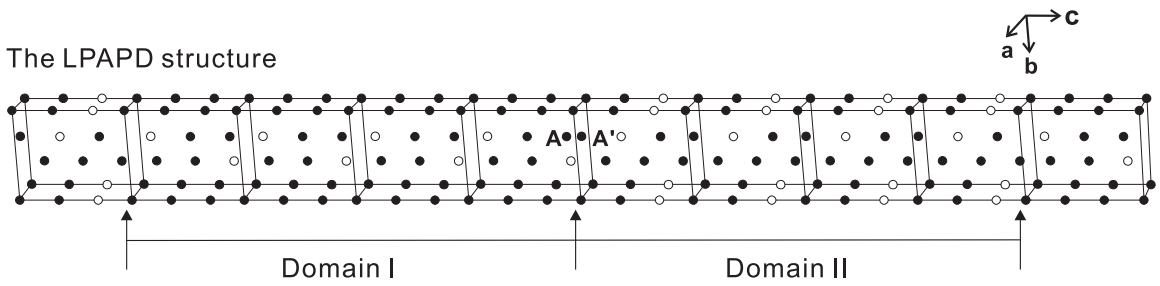


Figure 5.

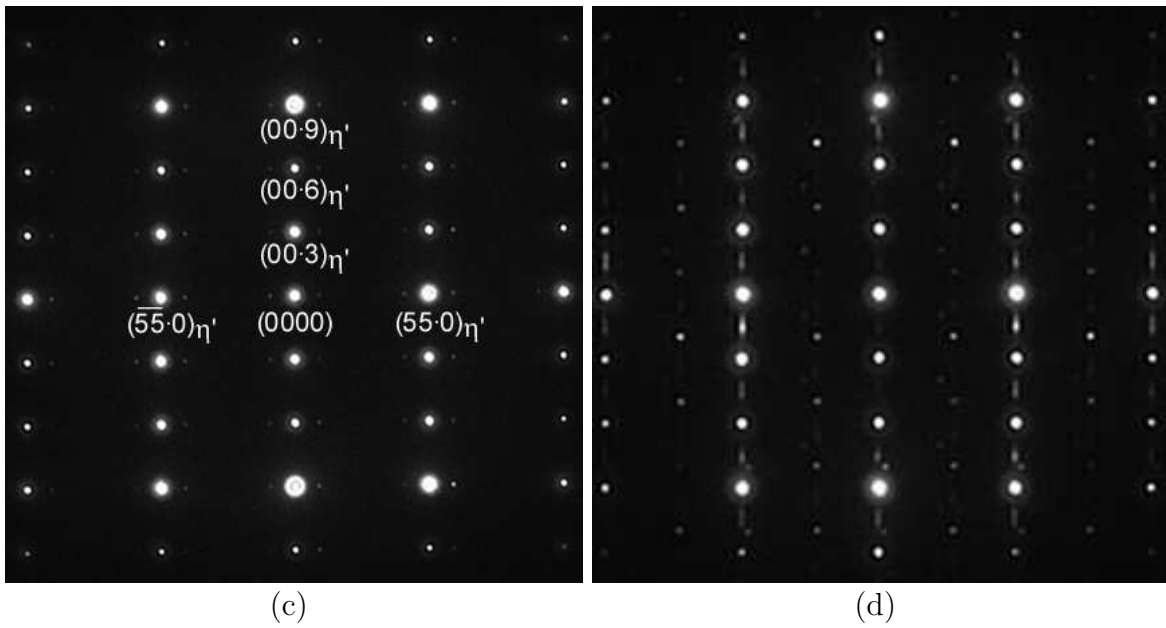
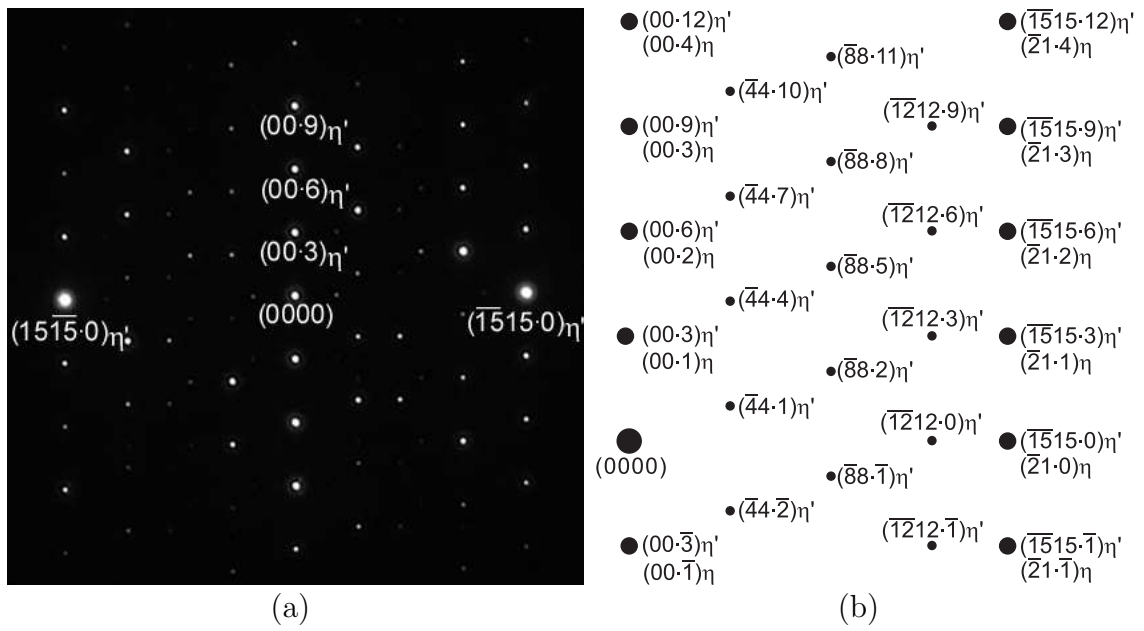


Figure 6.

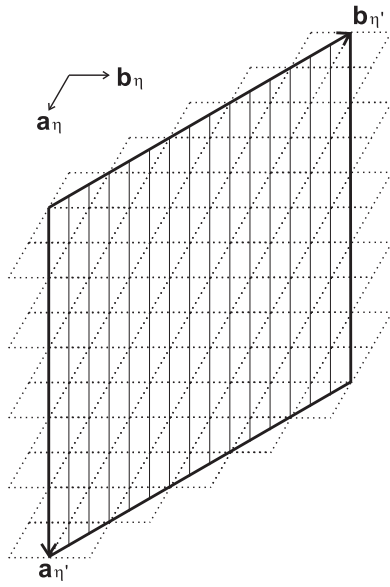
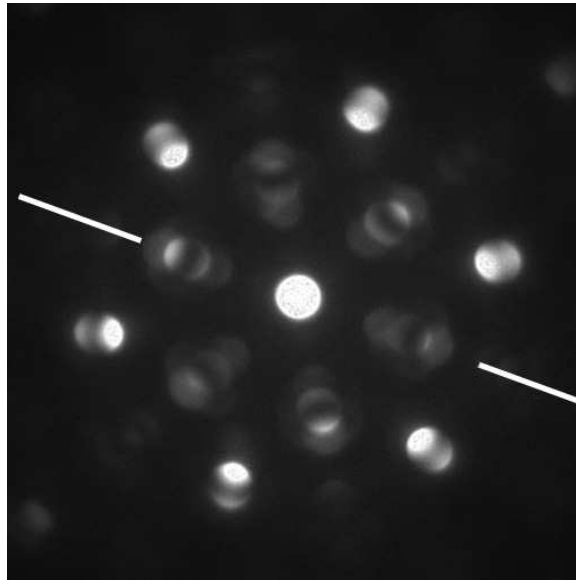
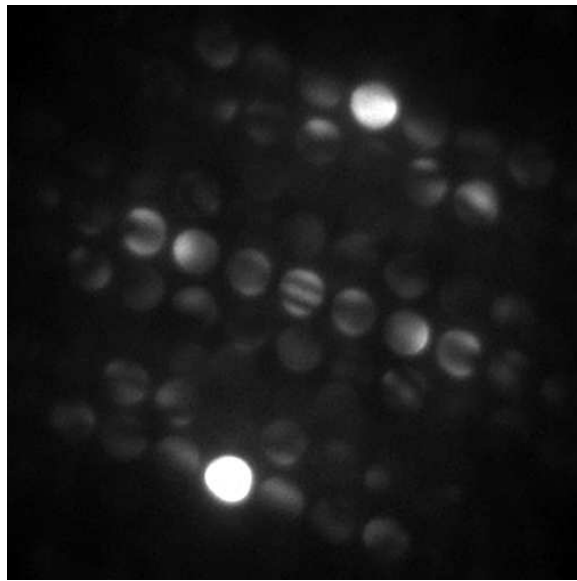


Figure 7.

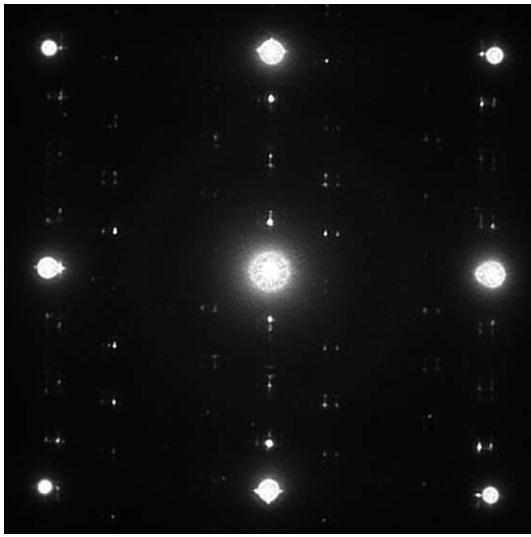


(a)

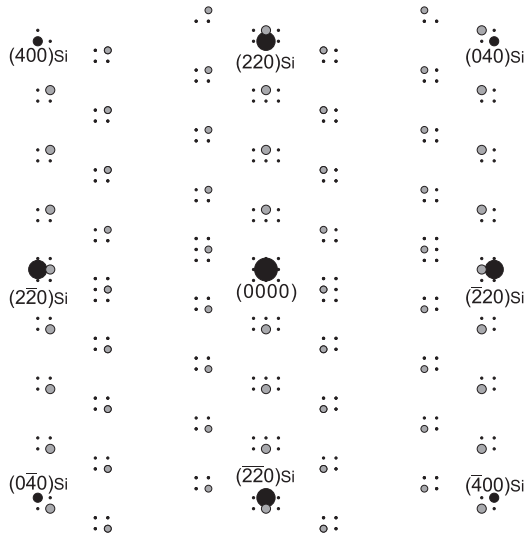


(b)

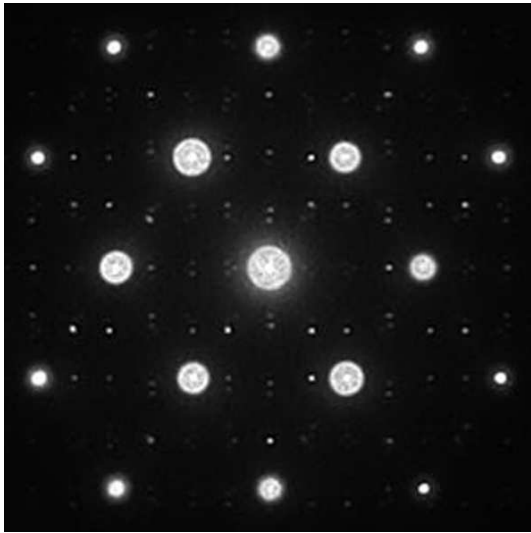
Figure 8.



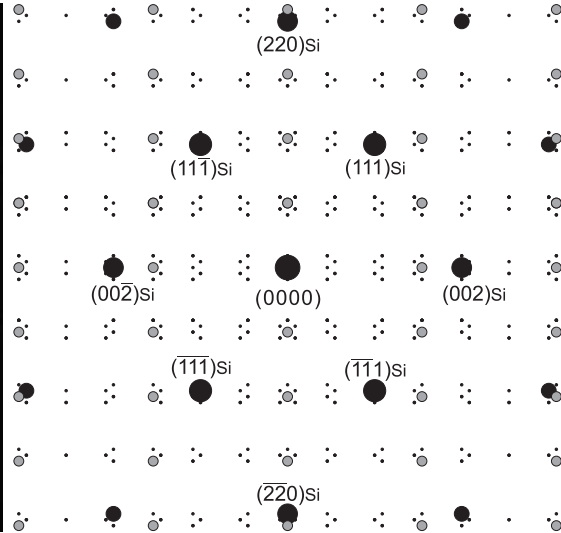
(a)



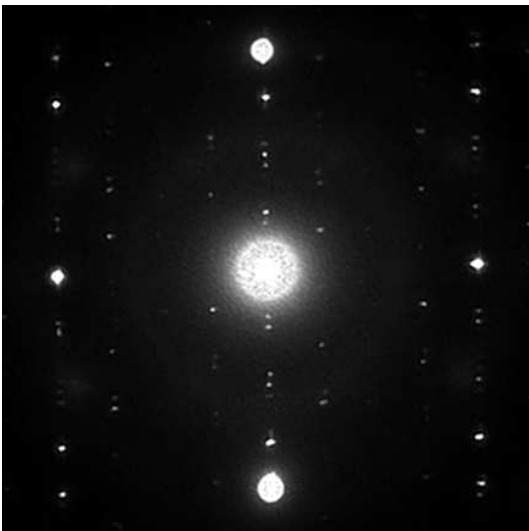
(b)



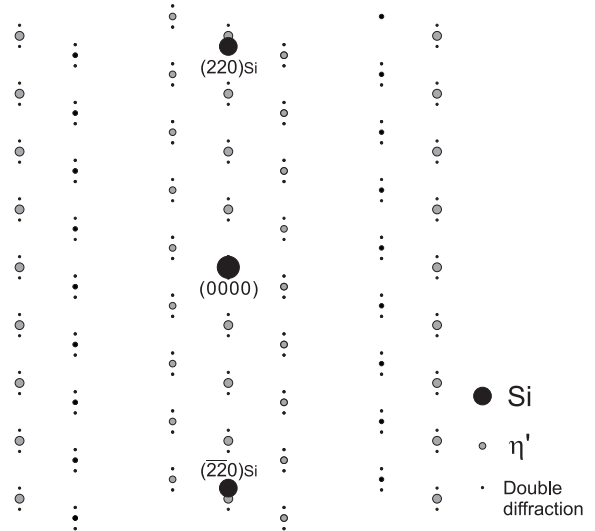
(c)



(d)



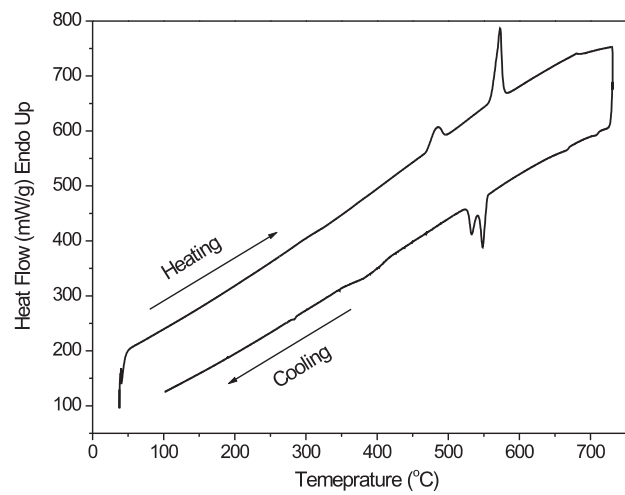
(e)



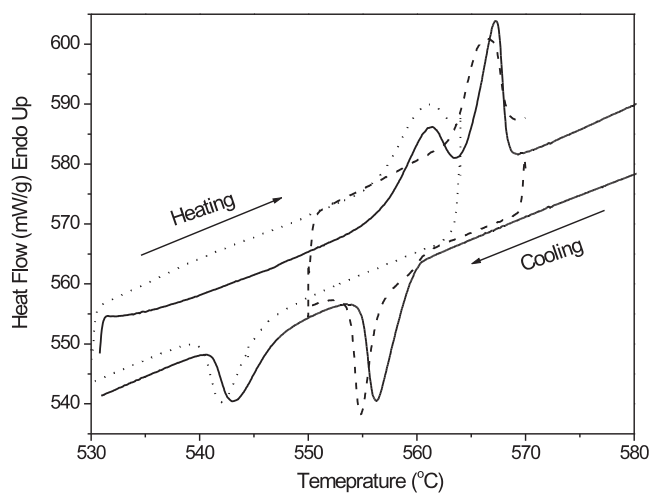
(f)

● Si
 ○ η'
 · Double diffraction

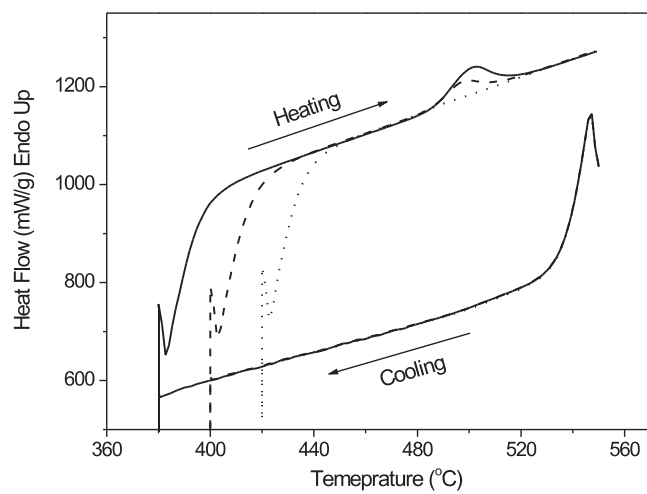
Figure 9.



(a)



(b)



(c)

Figure 10.

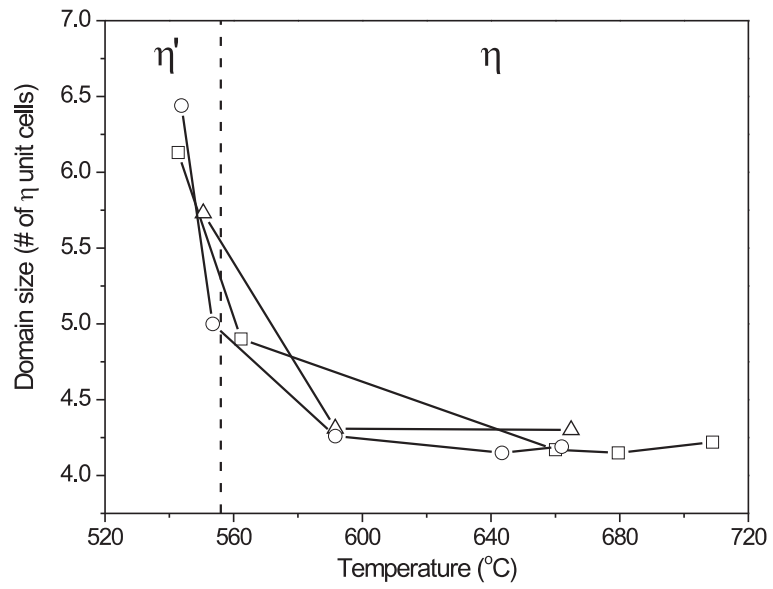


Figure 11.

Table 1. Relative intensities of the $(00\cdot l)_{SL}$ reflections of the LPAPD structure.

l	Structure in Fig. 5	With vacancies at the boundary	l	Structure in Fig. 5	With vacancies at the boundary
1	1.78	0.01	14	0	0.54
2	0	1.72	15	1.78	0.69
3	2.05	0.11	16	30.05	27.62
4	0	1.61	17	2.6	1.35
5	3.14	0.72	18	0	0.2
6	0	1.45	19	4.64	3.32
7	15.44	10.53	20	0	0.09
8	0	1.24	21	11.89	10.65
9	10.79	13.42	22	0	0.02
10	0	1.00	23	100	100
11	1.78	1.61	24	0	0
12	0	0.77	25	94.26	94.34
13	1.50	0.67			